

Article

# Visualizing and Evaluating Microbubbles in Multiphase Flow Applications

Safa A. Najim <sup>1</sup>, Deepak Meerakaviyad <sup>2</sup>, Kul Pun <sup>2</sup>, Paul Russell <sup>2</sup>, Poo Balan Ganesan <sup>3</sup>, David Hughes <sup>2</sup>  
and Faik A. Hamad <sup>2,\*</sup>

<sup>1</sup> Electrical Engineering Department, College of Engineering, Basrah University, Basrah 61004, Iraq; safa.najim@uobasrah.edu.iq

<sup>2</sup> School of Computing, Engineering & Digital Technologies, Teesside University, Tees Valley, Middlesbrough TS1 3BX, UK; d.meerakaviyad@tees.ac.uk (D.M.); k.pun@tees.ac.uk (K.P.); p.russell@tees.ac.uk (P.R.); d.j.hughes@tees.ac.uk (D.H.)

<sup>3</sup> Department of Mechanical Engineering, Faculty of Engineering, University Malaya, Kuala Lumpur 50603, Malaysia; poo\_ganesan@um.edu.my

\* Correspondence: f.hamad@tees.ac.uk

**Abstract:** Accurate visualization of bubbles in multiphase flow is a crucial aspect of modeling heat transfer, mixing, and turbulence processes. It has many applications, including chemical processes, wastewater treatment, and aquaculture. A new software, Flow\_Vis, based on experimental data visualization, has been developed to visualize the movement and size distribution of bubbles within multiphase flow. Images and videos recorded from an experimental rig designed to generate microbubbles were analyzed using the new software. The bubbles in the fluid were examined and found to move with different velocities due to their varying sizes. The software was used to measure bubble size distributions, and the obtained results were compared with experimental measurements, showing reasonable accuracy. The velocity measurements were also compared with literature values and found to be equally accurate.

**Keywords:** software; visualization; microbubble; laminar flow; turbulent flow



**Citation:** Najim, S.A.; Meerakaviyad, D.; Pun, K.; Russell, P.; Ganesan, P.B.; Hughes, D.; Hamad, F.A. Visualizing and Evaluating Microbubbles in Multiphase Flow Applications. *Fluids* **2024**, *9*, 58. <https://doi.org/10.3390/fluids9030058>

Academic Editor: Markus Klein

Received: 1 December 2023

Revised: 16 February 2024

Accepted: 17 February 2024

Published: 27 February 2024



**Copyright:** © 2024 by the authors. Licensee MDPI, Basel, Switzerland. This article is an open access article distributed under the terms and conditions of the Creative Commons Attribution (CC BY) license (<https://creativecommons.org/licenses/by/4.0/>).

## 1. Introduction

Fluid flow is a central subject in engineering, encompassing all traditional engineering disciplines. It holds significant importance across a wide array of contexts [1,2]. Research on gaseous fluxes contributes to the advancement of various technologies, including the design of machinery such as turbines and combustion engines, as well as the production of automobiles, aircraft, and spacecraft. Moreover, it plays a crucial role in civil engineering projects such as harbor design, modeling tidal and river flow patterns, and coastal area protection. In chemical engineering, understanding flow behavior in process equipment like reactors [3] and pipe networks is essential. Additionally, it finds application in medicine for modeling blood flow through arteries and veins.

While the flow of single-phase fluids is well understood, the dynamics of multiphase flow remain less so and are currently a focal point of research. Mass transfer processes involved in separators and reactors heavily rely on detailed knowledge of multiphase fluids, particularly the motion of droplets/bubbles in the continuous phase. New methods for determining droplet distribution and motion are scarce, and visualization-based techniques offer a promising direction.

A primary requirement for an accurate multiphase flow measurement technique is a high degree of temporal and spatial resolution, as the flow significantly varies over time and space. In comparison to probe techniques such as hot-film and optical probes employed in multiphase flow, visualization techniques offer several advantages, including minimal flow disturbance, quick response time, high visual resolution, and the ability to identify the

profile near the gas–liquid interface despite its limited thickness. This method can provide more precise information on void fraction, flow pattern, gas and liquid velocity, and bubble size and velocity through individual bubble tracking. Additionally, it can be utilized to calibrate sensors/probes used in industrial applications that cannot be visually monitored through transparent walls.

### 1.1. Fluid Flow Visualization

Flow visualization has existed alongside fluid flow studies for as long as fluid flow research has been conducted. Experimental flow visualization has been the primary method used in the study of fluid flow until quite recently [4]. The following are examples of reasons why experimental flow visualization techniques are utilized:

1. To gain insight into fluid movement around a scale model of a real object without the need for extensive calculations.
2. To inspire the development of new and improved theories of fluid flow.
3. To verify a new theory and test prototypes for new products.

Computer-generated visualization is a more recent innovation. It is used to represent complex data streams produced from mathematical models and simulations of flow systems. Often, the data produced are too complex and extensive to fully analyze as strings of numbers. It is widely accepted that the benefits of the growth in computing power will be greatly enhanced if the computer is not only used to calculate numerical data but also to visualize these facts in an understandable way [5,6]. Thus, information can be better comprehended when presented visually through pictures, graphs, and locus plots rather than numerically.

The data visualization acquired through modelling fluid flow can serve various purposes, depending on its context of use. The process of verifying and analyzing theoretical models is an essential component of fundamental research. Comparing the flow model being used to the “real” fluid flow is necessary whenever a flow phenomenon is represented by a model [7].

Calculating and visualizing flow using a model, as well as comparing the results with experimental data, are two approaches that can validate the correctness of the model. If numerical results and experimental flow are displayed similarly, qualitative verification through visual inspection can be highly effective.

Research into numerical methods for solving flow equations may be aided by visually representing the solutions found, as well as visually representing the intermediate study results obtained throughout the iterative solution process. This can be done both before and after finding the solution [8,9]. Visualizing fluid flow phenomena can be useful for design, optimization, and evaluation. Additionally, it can assist in designing any object functionally related to fluid flow.

Communication of flow analysis results to others, particularly those who are not professionals in the subject, is important [10]. This is especially true when communicating ideas to individuals who are not professionals in a specific industry.

### 1.2. Flow Visualization Procedures

In most cases, the visualization process consists of the following four stages: data importing, data filtering and enrichment, data mapping, and data rendering, as depicted diagrammatically in Figure 1. Step 1 involves locating a representation of the primary information to be investigated in the form of a data set, which can be either continuous or discrete in nature [10,11]. In practical terms, importing data entails selecting a specific implementation of a dataset and then converting the initial information to the representation implied by the selected dataset. This process should involve a one-to-one mapping or data copying.

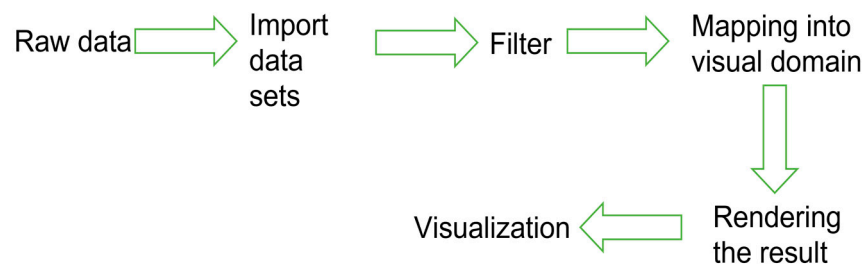


**Figure 1.** Data visualization process.

The second step of data visualization is termed data filtering and enrichment. It involves identifying the features or aspects of the data that require focus. In most cases, the imported data do not correspond one-to-one with the relevant aspects. The data are filtered to extract pertinent information and then enriched with higher-level data to aid in the specific task. This process generates an enriched dataset that directly represents the features of interest for the task at hand.

The third step entails mapping the dataset to the visual domain. This involves associating aspects of the visual domain with the data aspects included in the enriched dataset.

The rendering operation marks the conclusion of the visualization process. Rendering transforms the scene created by the mapping operation into two or three dimensions, adjusting various user-specified viewing parameters such as viewpoint and lighting to produce desired images. In typical visualization applications, viewing parameters are considered part of the rendering operation.

A functional description of this process can deepen understanding of the steps comprising the visualization process [12–15]. The visualization process in Equation (1) can be visualized as a function  $Vis$  that maps between the set of all possible types of raw input data, known as  $D_I$ , and the set of created images, known as  $V$  [16]:

$$Vis : D_I \rightarrow V \quad (1)$$

### 1.3. Flow Field Topology

Critical point theory serves as the foundation for flow topology analysis. This theory has been applied in various settings to examine the solution trajectories of ordinary differential equations. The topology of a vector field consists of critical points, where the velocity vector equals zero, as well as integral curves and surfaces connecting these critical points [17]. Visualizing the topology of a vector field can convey its topological properties without overwhelming the viewer with excessive information that is already known. To investigate and present vector field topologies, the following steps must be taken:

1. Identify the most important locations.
2. Classify the significant components of the situation.
3. Compute integral curves and surfaces.

### 1.4. Objectives of This Work

Currently, Teesside University is conducting experimental measurements for small droplets in three-phase separators on oil–water mixtures and for microbubbles in an air–water Venturi-type microbubble generator. Both of these applications require a methodology to measure the droplet/bubble size distribution and determine the velocities of individual droplets/bubbles. The results for these experiments are obtained as both still photographs and video footage. Consequently, the data files produced are large, particularly in the case of video footage containing moving images.

Computerized flow visualization is seen as a method of analyzing these images to convert pictures into numerical data files. From this, the velocity, size distribution, and number of droplets/bubbles in the continuous phase can be determined before transform-

ing the data into graphs and locus plots, allowing for more quantitative interpretation than is possible from video and still imagery alone. This technique makes information on the entire flow field readily comprehensible, offering numerous advantages, especially for moving images or large data files [18–21]. Notably, it eliminates the need for any data processing, which is a significant benefit [10]. One outcome of this research is the development of software capable of managing moving data; the bubbles investigated represent these data. Working with a video provides potential improvements in accuracy and the ability to measure velocity compared to working with discrete still imagery.

Applying computerized flow visualization to the systems measured by Teesside University poses challenges. Both water–air and water–oil–air are transparent fluid mixtures, making it difficult to visualize the flow field and detect bubbles/droplets traveling within it using visualization software.

The following section of this paper discusses a novel approach to the analysis of moving data using data visualization. The newly developed software (Flow\_Vis, <https://sites.google.com/view/flowvis/home>) was applied to analyze video-recorded experiments. During the experiment, the software successfully analyzed the bubbles present in the moving liquid in terms of size, number, and velocity.

## 2. Flow\_Vis Software

### 2.1. Generating the Bubbles

It is possible to use bubbles produced by a bubble generator in order to improve the perception of flow pattern. Clearer streamlines are produced from bubbles injected in the flow rather than smoke or solid particle dispersion because the bubbles are easier to differentiate from one another. Bubbles are able to accurately convey the characteristics of the flow because of their extremely low moments of inertia. One of the advantages of following individual bubbles is one way to locate streamlines, in the event that they are present.

Air bubbles, because of their low density and inert nature, can be formed and float through the liquid. This is made possible by the fact that air bubbles may be generated by any microbubble generator device such as a Venturi. Each bubble has a center of specific air volume that is enclosed in a layer of liquid. The mixing nozzle is the location where the bubbles are formed. The confined space in the throat is being traversed by the flow of air. The air is sucked into throat by the vacuum generated due the high velocity of liquid, which subsequently fills the space around the tube with air at a flow rate that has been previously specified. This is accomplished by passing the bubble film solution through the air that is contained in the central tube. When the bubbles are ready to be transported, low-pressure, dry compressed air is forced into the outer tube. This causes the bubbles to move forward.

Figure 2 shows the schematic diagram of the experimental apparatus used in this study to generate the microbubble field. The apparatus consists of the water tank (380 × 280 × 740 mm) connected to a circulation water pump via a water flow meter, a flow control brass ball valve, and Venturi microbubble generator. The maximum flow rate of the water pump is 13.3 L/m at pressure of 3.2 bar at the inlet of the Venturi microbubble generator. The Venturi is connected to the one of the tank walls where atmospheric air is sucked into its throat through an air flow meter followed by the air feed pipe. The Venturi is where the air is mixed with the main water flow.

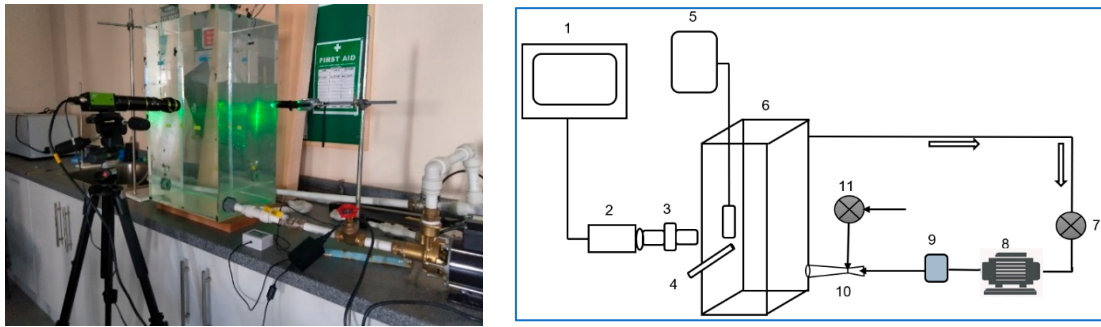


**Figure 2.** Schematic diagram of the experimental apparatus for microbubble generator. (1) Computer, (2) flow visualization camera, (3) microscopic lens, (4) laser lamp, (5) flow meter and thermometer, (6) water tank, (7) water flow meter, (8) water pump, (9) flow control brass ball valve, (10) Venturi microbubble generator, and (11) air flow meter.

### 2.2. Visualizing the Bubble Flow

The visualization procedure can be considered as a series of stages, each modelled by a different data transformation operation. Up until it produces the output visuals, the incoming data go through this process while being transformed in a variety of ways. In general, the bubble flow visualization process of data visualization can be viewed as a process with four stages: importing data sets, filtering, mapping, and rendering, as shown in Figure 1.

For the purpose of locating the bubbles in order to map them in visual space, a method known as the Hough circle transform is applied. This method begins with the presumption that the bubbles in the image are described as follows:

$$(x - a)^2 + (y - b)^2 = r^2 \tag{2}$$

Any edge point  $(x_i, y_i)$  in the  $(a, b, r)$  parameter space will be turned into a correct bubble if  $(a, b)$  is the coordinate of the bubble center and  $(r)$  is the radius of the bubble. If each of the image points is located on a different bubble, then the bubbles will collide at a single point in the coordinates  $(a, b, r)$  that correspond to the parameters of the bubble when all of the image points are located on the same bubble.

If the radii of the bubbles in a space are known, then the search can be simplified down to using only two dimensions. The  $(a, b)$  coordinates of the centers are the essential information needed.

$$x = a + r \cdot \cos(\theta) \tag{3}$$

$$y = b + r \cdot \sin(\theta) \tag{4}$$

The points in the parameter space denoted by the coordinates  $(a, b)$  lie on a bubble with a radius of  $r$  and its center at  $(x, y)$ . The real center point will be the same for all of the parameter bubbles, and it is possible to locate it, as in Figure 3.

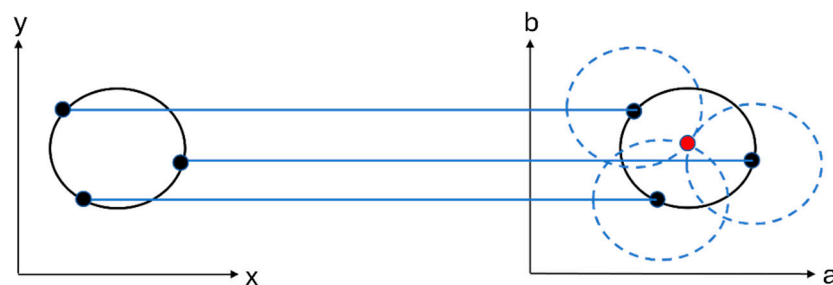


**Figure 3.** Every point in geometric space (left) produces a bubble in parameter space (right). The intersection of the bubbles in parameter space with the center of geometric space is  $(a, b)$ .

In an ideal situation, the center of the bubble would be situated on a line that is perpendicular to the path of the moving bubble. Moving along the normal of each edge point is consequently all that is required to determine the various places of the centers. The distance that separates each edge point from the anticipated center of that bubble is one measurement that might be used to approximate the size of the associated bubble's radius. Because the center of a bubble has to lie on the normal of each point on the bubble, the actual center of the bubble is the point at which all of these points cross. The source codes for this software can be obtained from the website in reference [22].

### 2.3. Bubbles Velocity

After the bubbles have been recognized, the next step is to identify their locations. To achieve this an approximation of the velocity field in the region surrounding the bubble  $X_p$  is obtained by applying a first order Taylor expansion. As a consequence of this, the velocity  $u$  can be determined by applying the formula that is presented below:

$$u_i = u_{p,i} + (x_j - x_{p,j}) \frac{\partial u_i}{\partial x_j} \tag{5}$$

The partial derivatives  $\Delta u = \frac{\partial u_i}{\partial x_j}$  completely specify the velocity field in the area surrounding the crucial point. A classification method for the bubble locations can be determined by using the eigenvalues and eigenvectors of  $u$ . A vector field can take on a variety of different configurations, including the following: Positive eigenvalues are representative of velocities that are moving away from the critical point, whereas negative eigenvalues are representative of velocities that are moving in the direction of the bubble. When a bubble has both negative and positive real values, then such a bubble can be moved without incurring either compression or expansion.

### 2.4. Dimension Reduction Visualization

Sometimes it is necessary to reduce a video of an experiment into a single image in order to watch the movement of the bubbles as they move throughout the experiment. Thus, this video may be reduced from  $D$  dimensions down to one dimension (where  $D \gg 1$ ), allowing us to have one visualization that goes in for the target to be achieved. In order to finish this procedure, it is necessary to use Equation (5), which will result in a reduction in the dimensions.

$$y_i \rightarrow y_j + \lambda(t) \cdot T(d_{ij}) \cdot \frac{r_{ij} - d_{ij}}{d_{ij} + \epsilon} \cdot (y_j - y_i) \tag{6}$$

$$T(d_{ij}) = \begin{cases} 1, & \text{if } (d_{ij} > d_c(t)) \text{ and } (d_{ij} > r_{ij}) \\ 0, & \text{otherwise} \end{cases} \tag{7}$$

where  $y_i$  is a point in the projection space,  $y_j$  is a point that needs to be updated (and is a neighboring point to  $y_i$ ),  $r_{ij}$  weight (distance) in the high dimension, and  $d_{ij}$  weight (distance) in the projection space, and  $\epsilon$  value is small to prevent dividing by zero and reduce varies depending on the data. The parameter  $d_c$  is a hypersphere's radius. The original distance  $r_{ij}$  in the video is being compared to the projected distance  $d_{ij}$  in the new location. The update is performed based on the value of the learning rate.

## 3. Experimental Results

The new software (Flow\_Vis) was developed in MATLAB following the methodology outlined in Section 2. The processing was performed on a computer running the Windows 11 operating system and equipped with an Intel Core i5 processor.

In the context of the present paper, accuracy, robustness, computational complexity, and storage were the key aspects to be evaluated. The accuracy of bubbles in synthetic images was assessed by comparing the absolute errors of the estimated diameter and center coordinates with the actual values of the bubble sizes.

The analysis of the results is divided into four stages:

1. The first stage explains how the video of the entire fluid movement is analyzed using Flow\_Vis.
2. In the second stage, each frame (or individual photo) is processed separately.
3. The third stage involves computing the velocity of the bubbles and visually illustrating it as droplet loci.
4. Finally, a dimension reduction technique is applied to condense the video into a single visualization of bubble loci.

### 3.1. Video Analyzing

To conduct a comprehensive analysis of the experimental data, a video recording was made while the microbubble generator was operating. The recorded video was subsequently analyzed using the Flow\_Vis software, and conclusions were drawn regarding the experiment's reliability. One notable feature that distinguishes this tool from others is its ability to handle lengthy video files. When recording the experiment, the video serves as input to the software, which then processes it to generate the most accurate visualization of the bubbles. Figure 4 illustrates that the video capturing the flow of bubbles through the liquid consists of a total of 239 frames.

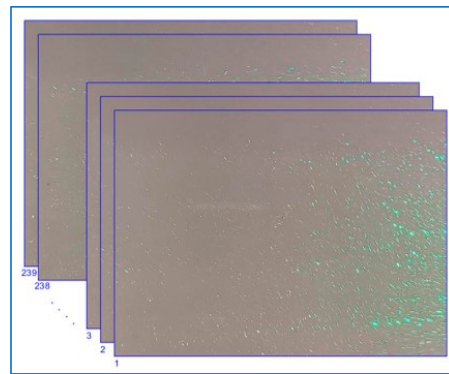


**Figure 4.** The video of an experiment has 239 frames.

In order to analyze the bubbles in this video comprehensively, it is necessary to examine all frames within the complete collection of available options. The sequential order of the frames in a video is crucial for accurate analysis and must be considered within the context of a specific evaluation. Figure 5 presents four graphs that assess each frame depicted in Figure 4. The software analyzes these frames based on the number of identified bubbles, with an average of 1488 bubbles recognized throughout the experiment.

In Table 1, the Flow\_Vis software analyzed the entire video, calculating the average diameter of the bubbles across all frames, which is 35 micrometers. The software will focus its attention on frame number 165, which exhibits the largest bubble diameter (39 micrometers), while frame number 33 has the smallest diameter for a bubble size (30 micrometers).

**Table 1.** Results of analysis of bubbles in fluid.

	Value	Frame No.
No. of Frames	239	
Mean of Bubble Diameter	35	
Mean of Bubble No.	1488	
Maximum Bubble Diameter	39	165
Minimum Bubble Diameter	30	33
Maximum No. of Bubbles	1744	45
Minimum No. of Bubbles	1151	193

Figure 5 presents the results of visualizing the video footage. In Figure 5a–c, the orange data represent the curve fit of the experimental data obtained from image processing software. Throughout the experiment, there was a noticeable change in both the total number of bubbles and their individual diameters, as depicted in Figure 5. Based on the information presented in Figure 5a, a significant number of bubbles were initially observed, which gradually decreased over time. Simultaneously, it was noted that the bubble diameters were very small at the beginning of the experiment but increased throughout the frame sequence, as shown in Figure 5b. This indicates that under these conditions, the bubbles are coalescing. Additionally, Figure 5c illustrates that the bubble diameter decreases as the bubble number increases, which is consistent with droplet coalescence.

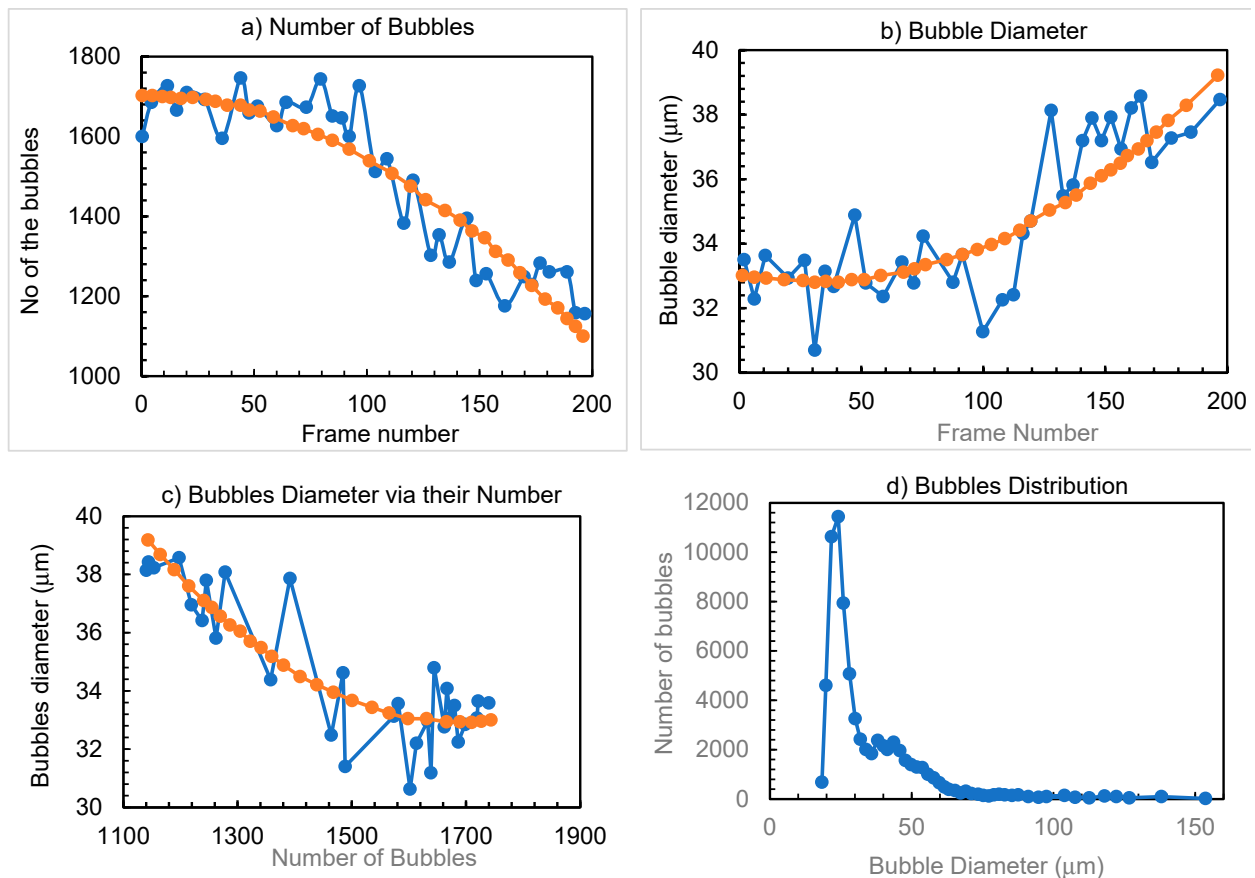


**Figure 5.** Analyzing the video to study the bubbles’ behavior. In (a–c), the orange data represent the curve fit of the experimental data from image processing software.

Figure 5d displays the bubble size distribution, revealing that the majority of the bubbles fall within a diameter range of 20–60 μm, with a peak number of bubbles at 35 μm.

An issue that may arise is how to address the location of certain bubbles. In this method, it is desired to project the relationships among three bubbles to accurately arrange their positions, as illustrated in Figure 3.

As evident from Figure 6a,b, frame 165 exhibits the largest bubble radius (39 micrometers), while frame 33 displays the smallest bubble radius (30 micrometers). This information, provided by Flow\_Vis, is crucial for supporting scientific research, as it aids specialized researchers in their identification efforts. Figure 6c,d indicate that frames 1 and 2 have the highest and lowest number of bubbles, respectively. These identified frames are significant as they are also utilized in Figure 5. Table 2 offers further insights and details on this aspect.

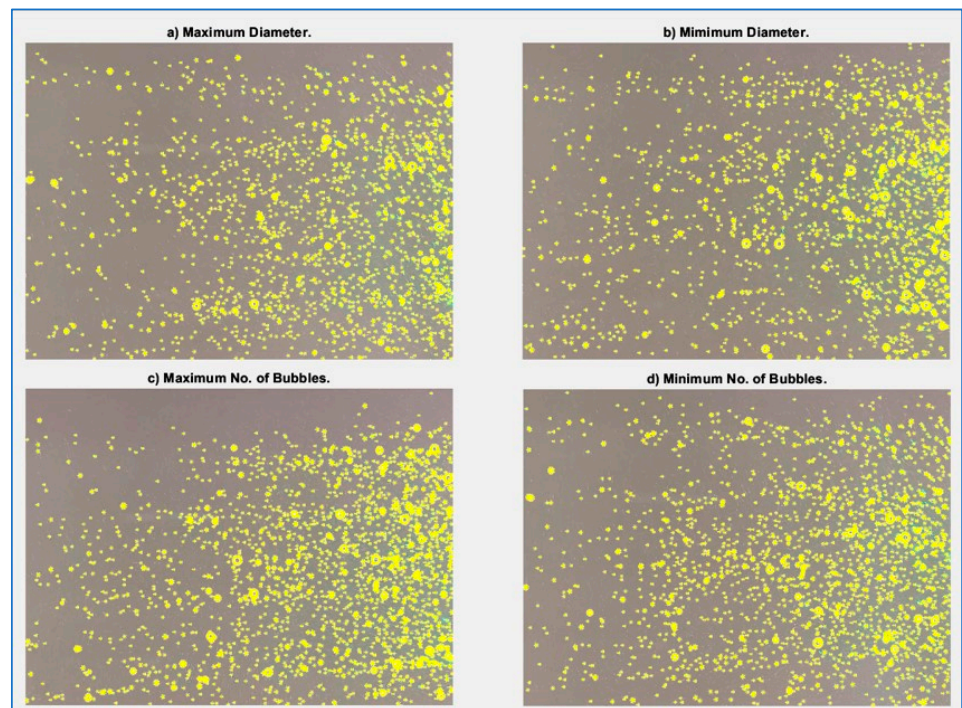


**Figure 6.** Frames which have maximum and minimum bubbles diameter and largest and smallest number of bubbles.

**Table 2.** The relation between the bubble size and their number for the selected frames.

Frame No.	No. of Bubbles	Diameter
33	1605	30
45	1744	34
165	1206	39
193	1151	38

The key findings from Figures 5 and 6 are summarized in Tables 1 and 2. It is evident from these figures that frame 45 contains the highest total number of bubbles, while frame 33 has the smallest bubble diameter. Hence, at the outset of the implementation process, the bubbles initially exhibit the characteristics of fluid flow bubbles. However, towards the end of the implementation, as depicted in frames 165 and 193, this situation is reversed, with the number of bubbles decreasing while their diameter increases. Figure 5c illustrates the relationship between bubble diameter and number, indicating a decrease in the number of bubbles as their size increases, and vice versa.

### 3.2. Data Analysis

After analyzing the video and locating the frames that are likely to play a significant part in the analysis, the Flow\_Vis software gives the user the option to investigate any individual frame. For instance, frame number 165 was selected for further interrogation, because it has an adequate number of bubbles with the largest diameter. Figure 7 depicts the selected frame alongside the recognized bubbles, totaling 1206 as in Tables 1 and 2. Despite demonstrating an average bubble diameter of 39 micrometers, Figure 7 presents the size distribution of all bubbles in this frame. The orange line represents the data from this work, plotted against the results from standard image processing software in blue. Once again, a strong correlation is observed between both datasets.

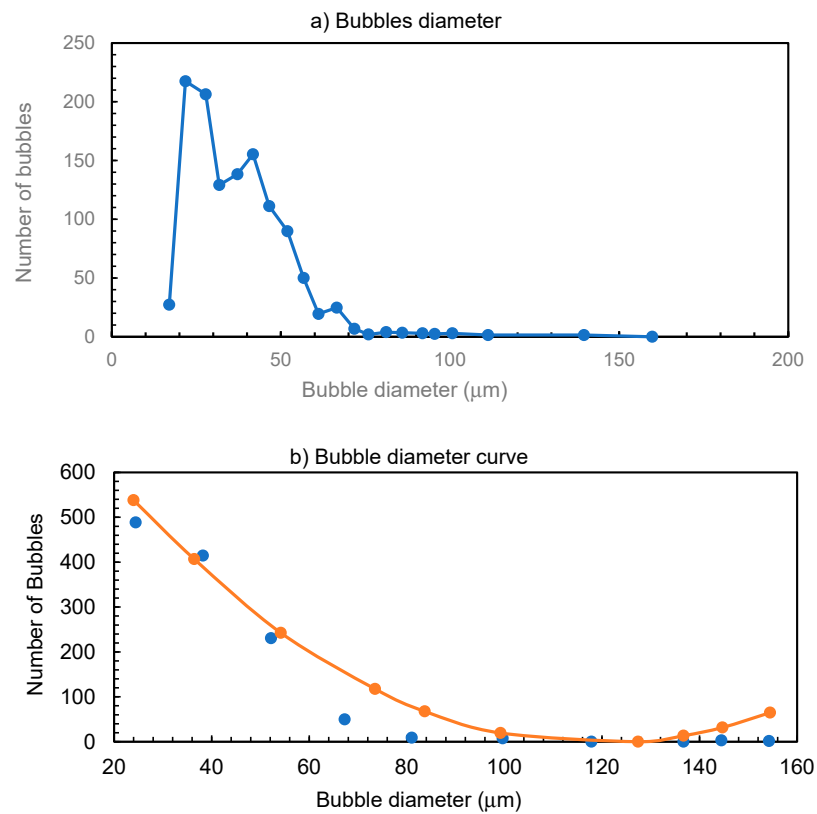


Figure 7. The results of analysis of frame 165.

The proposed software can handle samples by identifying a specific region containing the bubbles required for the study. Figure 8 illustrates the enlargement of the selected region, enabling a more focused examination of the bubbles to obtain more accurate observations and conclusions.

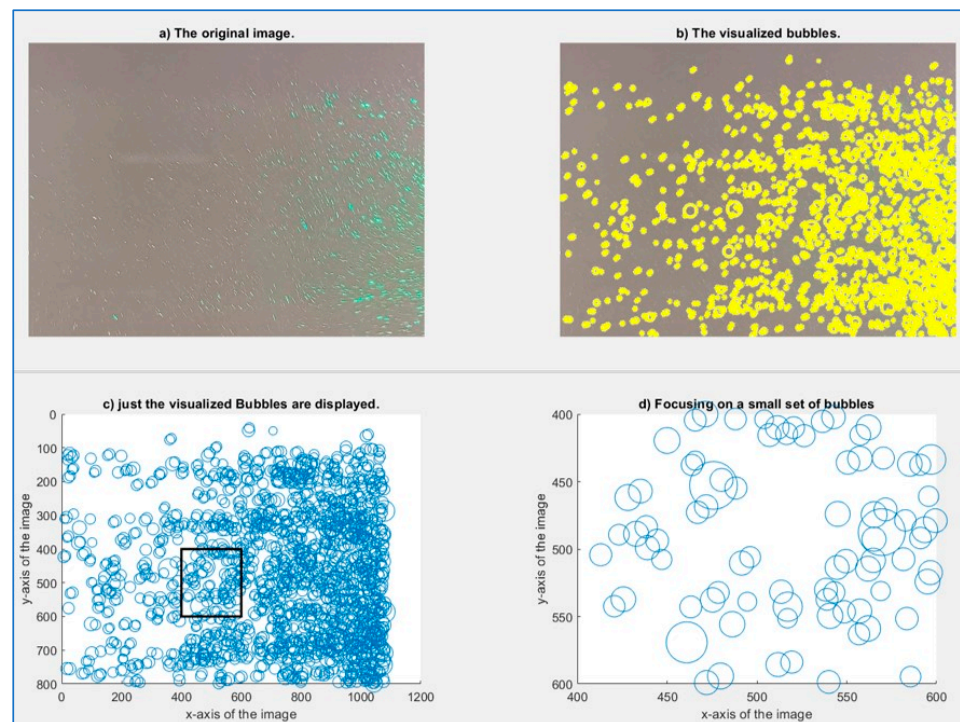
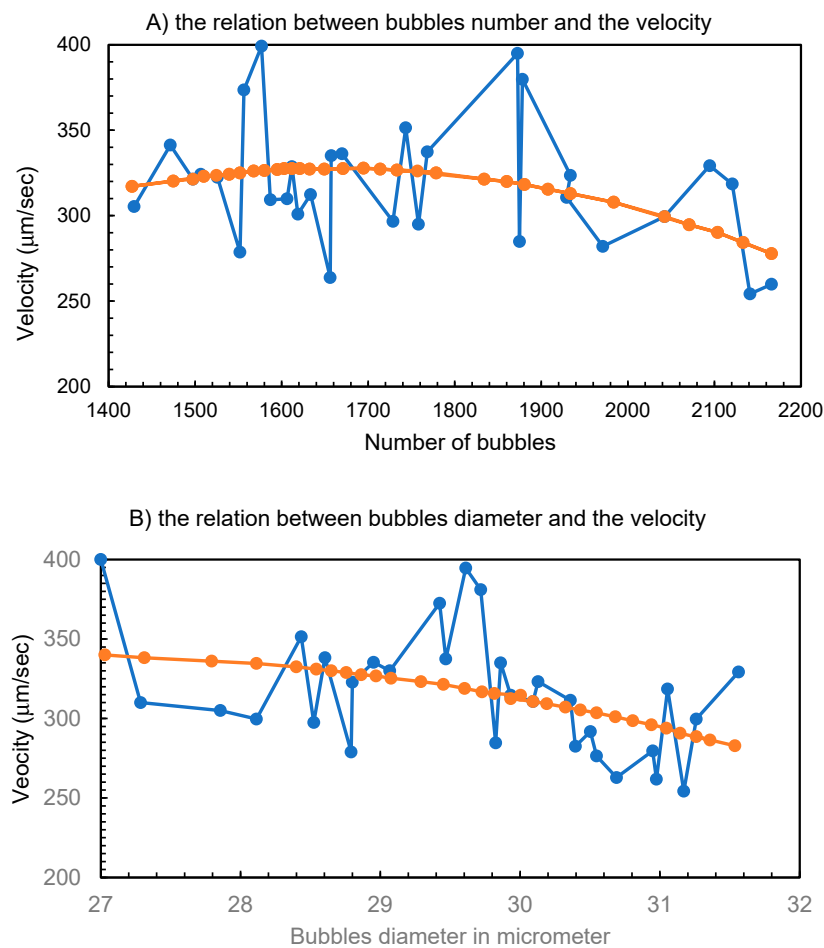


Figure 8. A sample of the visualized bubbles is taken from (b), and then they are enlarged and analyzed in great detail in (c).

The proposed software is able to deal with samples by selecting a particular region that contains bubbles that are required for the study. Figure 8 shows that the selected region is made larger, and a more concentrated study of the bubbles is carried out in order to obtain observations and draw conclusions that are more accurate.

### 3.3. Bubble Velocity

It is essential to understand the velocity of bubbles in a fluid and the direction in which they move. The Flow\_Vis software was capable of deriving these measurements from the recorded video, which is not achievable with standard image processing of still photography. Specifically, it provided a visualization illustrating the relationships among bubble velocity, diameter, and their number, demonstrating the movement of bubbles in relation to speed, as depicted in Figure 9. Upon examining Figure 9A, a direct correlation between bubble velocities and the number of bubbles is evident. The velocity of the bubbles is observed to decrease as the number of bubbles increases. This behavior can be attributed to changes in drag force and virtual forces with higher numbers of bubbles. Figure 9B indicates a decrease in bubble velocity with increasing bubble diameter, contrary to the physics of the flow. This discrepancy may be due to the short duration of data recording or an unknown error. Nonetheless, Figure 8 confirms that the velocity values are within expected ranges, and the Flow\_Vis software successfully identified this relationship.



**Figure 9.** Relation between bubble velocity with their number and diameter.

### 3.4. Dimension Reduction Visualization

When the theory of dimension reduction is applied to a fluid that is moving and contains bubbles, a great deal of information may be derived about the system. We observe

the degree of attention on the presence of these bubbles, and this is what is noticeable in Figure 10 when applying Equation (5) to reduce the dimensions from 239 to 1.



**Figure 10.** A reduced visualization of the 239 frames to one, which shows the bubbles flow in a whole processing.

The presence of white locations, in Figure 10, demonstrates that bubbles are being recorded from those locations, and an increase in the intensity of white indicates that bubbles are continuously present in those areas. Inversely, the darkness indicates that the bubbles are crossing in a short amount of time, and the length of time that they are present decreases as the darkness increases.

#### 4. Limitation

One limitation of the method is the inability to analyze changes in bubbles while they are not in motion. In such cases, the system can only study a single image, making it difficult to observe any changes occurring in the bubbles. Consequently, the size of the bubble remains constant. However, the likelihood of this is low, as the bubble is filled with air, which facilitates its movement within the surrounding liquid.

#### 5. Conclusions

The Flow\_Vis software, with the ability to analyze both video and still images to extract data, has been developed. The software has been tested against real experimental data generated from injection of air microbubbles into a tank of water. The Flow\_Vis software results were compared with data produced from experimental measurements made from still photography processed using conventional image processing techniques.

This comparison demonstrated that the software can accurately calculate the distribution of bubble sizes and the average diameter of bubbles. Further analysis was performed to compare bubble velocities generated from CFD models of the experiments with the Flow\_Vis generated velocities. Again, the results were found to agree well.

Experimental studies have demonstrated that this software possesses the ability to recognize bubbles even under challenging circumstances that provide difficulties for identification. Furthermore, it had the capability to analyze the bubbles from various perspectives, ascertaining their dimensions, velocity, and flow direction.

**Author Contributions:** Conceptualization, S.A.N., P.R., P.B.G., D.H. and F.A.H.; Methodology, F.A.H.; Software, S.A.N.; Validation, K.P. and P.R.; Investigation, D.M., K.P. and F.A.H.; Resources, P.B.G.; Data curation, D.M. and K.P.; Writing—original draft, S.A.N.; Writing—review & editing, F.A.H.; Visualization, S.A.N.; Supervision, P.R. and D.H.; Funding acquisition, P.B.G. and F.A.H. All authors have read and agreed to the published version of the manuscript.

**Funding:** This research received no external funding.

**Data Availability Statement:** Data are contained within the article.

**Conflicts of Interest:** The authors declare no conflict of interest.

## References

1. Ishii, K.; Aizawa, R.; Fumoto, K. Two-Dimensional Flow Field Visualization of Temperature Sensitive Magnetic Fluids Using a Luminescent Microcapsule. *IEEE Magn. Lett.* **2020**, *11*, 1–5. [[CrossRef](#)]
2. Zainudin, S.A.; Said, A.M.; Sulaiman, S. Visualization of fluid flow: Preliminary analysis. In Proceedings of the 2010 International Symposium on Information Technology, Kuala Lumpur, Malaysia, 15–17 June 2010; pp. 1–4.
3. Bucaro, A.; Murphy, C.; Ferrier, N.; Insley, J.; Mateevitsi, V.; Papka, M.E.; Rizzi, S.; Tan, J. Instrumenting Multiphysics Blood Flow Simulation Codes for In Situ Visualization and Analysis. In Proceedings of the 2021 IEEE 11th Symposium on Large Data Analysis and Visualization (LDAV), New Orleans, LA, USA, 25 October 2021; pp. 88–89.
4. Kubotera, H.; Kong, D.-W.; Song, Y.; Tokumiya, T.; Kim, C.-S. Computational Fluid Dynamics and Experimental Visualization of Time-Variable Air Flow Pattern Inside Hard Disk Drives. *IEEE Trans. Magn.* **2012**, *48*, 2395–2398. [[CrossRef](#)]
5. Xiaoxia, L.; Yafei, Y.; Pengtao, J. A Visualization Method Based on Discrete Flow Field Continuity Problem. In Proceedings of the 2018 IEEE 9th International Conference on Software Engineering and Service Science (ICSESS), Beijing, China, 23–25 November 2018; pp. 241–244.
6. Johnson, G.P.; Calo, V.M.; Gaither, K.P. Interactive Visualization and Analysis of Transitional Flow. *IEEE Trans. Vis. Comput. Graph.* **2008**, *14*, 1420–1427. [[CrossRef](#)] [[PubMed](#)]
7. Gaither, K. Visualization's role in analyzing computational fluid dynamics data. *IEEE Comput. Graph. Appl.* **2004**, *24*, 13–15. [[CrossRef](#)] [[PubMed](#)]
8. Cai, S.; Liang, J.; Gao, Q.; Xu, C.; Wei, R. Particle Image Velocimetry Based on a Deep Learning Motion Estimator. *IEEE Trans. Instrum. Meas.* **2020**, *69*, 3538–3554. [[CrossRef](#)]
9. Kang, K.; Chevray, R. Visualization of fluid mixing in microchannels. *IEEE Comput. Graph. Appl.* **2005**, *25*, 16–20. [[CrossRef](#)] [[PubMed](#)]
10. Najim, S.A.; Lim, I.S. Trustworthy dimension reduction for visualization different data sets. *Inf. Sci.* **2014**, *278*, 206–220. [[CrossRef](#)]
11. Schmitt, E. The Art of Data Visualization. In *Big Data: An Art of Decision Making*; Wiley: Hoboken, NJ, USA, 2020; pp. 187–217.
12. Wu, H.-M.; Kao, C.-H.; Chen, C.-H. Dimension Reduction and Visualization of Symbolic Interval-Valued Data Using Sliced Inverse Regression. In *Advances in Data Science: Symbolic, Complex, and Network Data*; Wiley: Hoboken, NJ, USA, 2020; pp. 49–77.
13. Balusamy, B.; Abirami, R.N.; Kadry, S.; Gandomi, A.H. Big Data Visualization. In *Big Data: Concepts, Technology, and Architecture*; Wiley: Hoboken, NJ, USA, 2021; pp. 293–346.
14. Najim, S.A.; Lim, I.S.; Wittek, P.; Jones, M.W. FSPE: Visualization of Hyperspectral Imagery Using Faithful Stochastic Proximity Embedding. *IEEE Geosci. Remote Sens. Lett.* **2015**, *12*, 18–22. [[CrossRef](#)]
15. Najim, S.A.; Najim, A.A.; Lim, I.S.; Saeed, M. Parallel faithful dimensionality reduction to enhance the visualization of remote sensing imagery. *Neurocomputing* **2015**, *168*, 560–565. [[CrossRef](#)]
16. Najim, S.A.; Ahmed, B.Y. Insightful visualization of remote sensing images. *IEEE Geosci. Remote Sens. Lett.* **2022**, *20*, 1–4. [[CrossRef](#)]
17. Kazakoff, M. CHAPTER 6: Structure Your Data (So Others Can Follow It). In *Persuading with Data: A Guide to Designing, Delivering, and Defending Your Data*; MIT Press: Cambridge, MA, USA, 2022; pp. 126–166.
18. Nsonga, B.; Niemann, M.; Fröhlich, J.; Staib, J.; Gumhold, S.; Scheuermann, G. Detection and Visualization of Splat and Antisplat Events in Turbulent Flows. *IEEE Trans. Vis. Comput. Graph.* **2020**, *26*, 3147–3162. [[CrossRef](#)] [[PubMed](#)]
19. Hobson, T.; Hammer, J.; Provins, P.; Huang, J. Interactive Visualization of Large Turbulent Flow as a Cloud Service. *IEEE Trans. Cloud Comput.* **2023**, *11*, 263–277. [[CrossRef](#)]
20. Han, G.; Chen, S.; Su, S.; Huang, Y.; Liu, B.; Sun, H. A review and perspective on micro and nanobubbles: What They Are and Why They Matter. *Miner. Eng.* **2022**, *189*, 107906. [[CrossRef](#)]
21. Patel, A.K.; Singhania, R.R.; Chen, C.-W.; Tseng, Y.-S.; Kuo, C.-H.; Wu, C.-H.; Di Dong, C. Advances in micro- and nano bubbles technology for application in biochemical processes. *Environ. Technol. Innov.* **2021**, *23*, 101729. [[CrossRef](#)]
22. Available online: <https://sites.google.com/view/flowvis/home> (accessed on 7 March 2023).

**Disclaimer/Publisher's Note:** The statements, opinions and data contained in all publications are solely those of the individual author(s) and contributor(s) and not of MDPI and/or the editor(s). MDPI and/or the editor(s) disclaim responsibility for any injury to people or property resulting from any ideas, methods, instructions or products referred to in the content.